

Water Resources Research

RESEARCH ARTICLE

10.1029/2018WR023568

Key Points:

- We proposed a data assimilation framework for a high-precision 2-D hydrodynamic model (HydroM2D) based on a modified PF method
- The PF-based data assimilation (PFDA) method for the HydroM2D model considered the spatial-temporal variability of Manning's roughness coefficient
- The PF-based data assimilation could simultaneously improve the performances of the HydroM2D in simulating water stages at all gauges

Correspondence to:

Y. Ye,
yeyuntao@iwhr.com

Citation:

Cao, Y., Ye, Y., Liang, L., Zhao, H., Jiang, Y., Wang, H., et al (2019). A modified particle filter-based data assimilation method for a high-precision 2-D hydrodynamic model considering spatial-temporal variability of roughness: Simulation of dam-break flood inundation. *Water Resources Research*, 55, 6049–6068. <https://doi.org/10.1029/2018WR023568>

Received 29 JUN 2018

Accepted 21 JUN 2019

Accepted article online 2 JUL 2019

Published online 25 JUL 2019

A Modified Particle Filter-Based Data Assimilation Method for a High-Precision 2-D Hydrodynamic Model Considering Spatial-temporal Variability of Roughness: Simulation of Dam-Break Flood Inundation

Yin Cao^{1,2}, Yuntao Ye¹ , Lili Liang¹, Hongli Zhao¹, Yunzhong Jiang¹, Hao Wang^{1,2}, Zhenyan Yi¹, Yizi Shang¹, and Dengming Yan^{1,2}

¹Department of Water Resources, China Institute of Water Resources and Hydropower Research, Beijing, China, ²College of Environmental Science and Engineering, State Environmental Protection Engineering Center for Pollution Treatment and Control in Textile Industry, Donghua University, Shanghai, China

Abstract The particle filter-based data assimilation method is an effective tool to adjust model states based on observations. In this study, we proposed a modified particle filter-based data assimilation method with a local weighting procedure (MPFDA-LW) for a high-precision two-dimensional hydrodynamic model (HydroM2D) in dam-break flood simulation. Moreover, a particle filter-based data assimilation method with a global weighting procedure (PFDA-GW) for the HydroM2D model was also investigated. The MPFDA-LW and the PFDA-GW for the HydroM2D model, respectively, adopted spatially nonuniform and uniform Manning's roughness coefficients. The MPFDA-LW considering spatial-temporal variability of Manning's roughness coefficient could significantly improve the performances of the HydroM2D model in simulating water stages at all gauges simultaneously, whereas the PFDA-GW considering temporal variability of Manning's roughness coefficient could only slightly improve the performances of the HydroM2D model in simulating water stages at a few gauges. The MPFDA-LW is more suitable for improving the performance of 2-D hydrodynamic models in flood inundation simulation than the PFDA-GW.

1. Introduction

To date, a large number of reservoirs have been built on natural rivers for the purposes of flood control, power generation, irrigation, water supply, navigation, tourism, and fishery (S. Zhang et al., 2017). Although the safety of reservoirs has been continuously improved, dam-break problems occur from time to time due to overcrowding, damage to dam foundations, earthquakes, and human factors (Marsooli & Wu, 2014). Rapid flows resulting from dam-break may cause devastating damage to the environment and huge losses to life and property (Penna et al., 2013). The accurate simulation of the characteristics of water flow such as water stage, discharge, arrival time, and duration during dam-break flood inundation is important for dam-break risk prediction and disaster assessment (Mao et al., 2016).

Hydrodynamic models are effective tools to simulate water flows in natural and artificial water systems and have been widely used in real-time flood forecasting (Xu et al., 2017), dam-break flow simulation (Ye & Zhao, 2017), and sediment transport and water quality prediction (Camacho et al., 2015; Coraci et al., 2007). Water stages and discharges of dam-break flood often experience drastic changes within a short period (Aureli et al., 2000), so the hydrodynamic model with a high performance is required for accurately simulating dam-break flood inundation. The performances of hydrodynamic models depend on the precision of model parameters (e.g., Manning's roughness coefficient), model inputs (e.g., initial and boundary conditions such as inflow hydrograph and river-bed geometry), and model structures (e.g., governing equations and numerical computation method; Teng et al., 2017). Tiny errors in model parameters (Warmink et al., 2010), model inputs (Rueda et al., 2009), and model structures (Sehnert et al., 2009) may result in huge output errors. The uncertainties associated with model parameters, inputs, and model structures jointly result in the output uncertainty of hydrodynamic models.

The data assimilation approach can reduce the uncertainty of hydrodynamic model outputs through integrating observations and have been widely concerned (Giustarini et al., 2011; J. Neal et al., 2009; Qi

et al., 2014). The Ensemble Kalman Filter (EnKF) and its variants are common methods integrating observations with hydrodynamic models (Biancamaria et al., 2011; K. Kim et al., 2014; Schneider et al., 2018). The EnKF has a significant assumption that the prior distribution of model states is a multivariate Gaussian distribution. However, the assumption is generally invalid in nonlinear hydrodynamic models (Pasetto et al., 2012). The particle filter (PF) can relax the assumption (Moradkhani et al., 2005) and has been applied in hydrodynamic model assimilations (Giustarini et al., 2011; Y. Kim et al., 2013; Matgen et al., 2010; Xu et al., 2017).

PF-based data assimilation methods for hydrodynamic models involve two typical particle weighting procedures, namely, global weighting procedure and local weighting procedure (Giustarini et al., 2011). The PFDA-GW can obtain the global optimal estimation of water stages at all cross sections (Giustarini et al., 2011), but it is difficult to obtain the optimal estimation at each cross section with the PFDA-GW due to local systematic errors (Xu et al., 2017). On the contrary, the PFDA-LW can obtain the optimal estimation at each cross section and is more suitable for assimilating observations with a high accuracy into a hydrodynamic model that cannot be well calibrated (Giustarini et al., 2011).

Manning's roughness coefficient is a comprehensive coefficient indicating the resistance of water flow caused by underlying surface. It significantly affects the performance of hydrodynamic model in simulating and predicting water stages and discharge of flood inundation (Camacho et al., 2015; Chávarri et al., 2013; Thompson et al., 2008). Manning's roughness coefficients in hydrodynamic models are related to flow conditions, geography, and vegetation cover at cross sections or grid cells (Xu et al., 2017). Due to the longitudinal and transverse variations of the physical characteristics of a channel and the unsteady dam-break flood flow, both spatial and temporal variations of the Manning's roughness coefficients in the hydrodynamic model should be considered (Xu et al., 2017).

The study aims to develop a modified particle filter-based data assimilation method with a local weighting procedure (MPFDA-LW) for a 2-D hydrodynamic model (HydroM2D) considering the temporal-spatial variability of Manning's roughness coefficient. In the study, we explored the performance of the MPFDA-LW for the HydroM2D model in simulating and predicting dam-break flood inundation with the physical model of Toce River. In addition, the performance of the PFDA-GW was investigated. The remaining part of the paper is arranged as follows. The MPFDA-LW for the HydroM2D and validation case are introduced in section 2. Section 3 demonstrates the advantages of the MPFDA-LW for 2-D hydrodynamic models and discusses the potential of the MPFDA-LW for hydrodynamic models in flood prediction. Brief conclusions are finally drawn in section 4.

2. Materials and Methods

2.1. Hydrodynamic Models

Hydrodynamic models are mathematical models for simulating water movements. According to spatial representations of water flow, hydrodynamic models can be divided into one-dimensional (1-D), two-dimensional (2-D), and three-dimensional (3-D) models. The 1-D models are usually used to simulate flood inundation in confined river channels or pipes based on the assumption that the velocity distribution is uniform in the whole cross section. The 2-D models can provide detailed information on flood inundation in a two-dimensional space, such as the water area and spatial distributions of water depth and velocity. The 2-D models are applicable to simulate water inundation in a two-dimensional space when the third-dimensional water depth is shallow compared to the other two dimensions (Teng et al., 2017). In this situation, it is not necessary to adopt complex 3-D hydrodynamic models. In this study, a high-precision 2-D hydrodynamic model (HydroM2D; Cao et al., 2017) was adopted to simulate dam-break water flows and depth-averaged Navier-Stokes equations were used as the governing equations:

$$\frac{\partial(\zeta)}{\partial t} + \frac{\partial(\mathbf{u}h)}{\partial x} + \frac{\partial(\mathbf{v}h)}{\partial y} = 0, \quad (1)$$

$$\frac{\partial(\mathbf{u}h)}{\partial t} + \frac{\partial(\mathbf{u}^2h)}{\partial x} + \frac{\partial(\mathbf{u}\mathbf{v}h)}{\partial y} = -\frac{\tau_{bx}}{\rho} - gh \frac{\partial \zeta}{\partial x}, \quad (2)$$

$$\frac{\partial(\mathbf{v}h)}{\partial t} + \frac{\partial(\mathbf{u}\mathbf{v}h)}{\partial x} + \frac{\partial(\mathbf{v}^2h)}{\partial y} = -\frac{\tau_{by}}{\rho} - gh\frac{\partial\zeta}{\partial y}, \quad (3)$$

where ζ is the relative free water stage; $h = \zeta + h_s$ is the total water depth; h_s is the still water depth; \mathbf{u} and \mathbf{v} , respectively, represent the depth-averaged flow velocity components in the x and y directions; g is the gravitational acceleration; ρ is the water density; and τ_{bx} and τ_{by} are the bed friction stresses in the x and y directions, respectively.

In the HydroM2D model, equations (1)–(3) are numerically solved with the finite volume method. In the finite volume method, the governing equations are solved in an integral form. The method can maintain the conservative properties of numerical solutions (Q. Liang et al., 2004). We adopted the HLLC's approximate Riemann solution to compute the flow flux based on the two-dimensional shallow water equations (Q. Liang & Borthwick, 2009). The spatial and temporal precisions of the model were increased to the second-order precision by the MUSCL Hancock method (Q. H. Liang & Borthwick, 2009; Q. H. Liang et al., 2007). Slope source terms and friction source terms were discretized in order to ensure the model stability. A local bed modification method was introduced to efficiently and accurately simulate the movement of wet/dry fronts and water flow characteristics in complex terrains with irregular boundaries.

2.2. Particle Filter-Based Data Assimilation for the HydroM2D Model

The Kalman Filter (KF) is a widely used sequential data assimilation method. Prediction and analysis equations of the traditional standard KF method for hydrodynamic modeling can be expressed as equations (4) and (5). The EnKF were developed based on the KF by generating several ensemble members and adding perturbations. Equations (4)–(6) can be applied in each ensemble member and the forecast and analysis update equations for the EnKF are equations (7)–(9) (Burgers et al., 1998):

$$\mathbf{x}_{t+1}^f = f(\mathbf{x}_t^a, \theta_{t+1}, \mathbf{u}_{t+1}), \quad (4)$$

$$\mathbf{x}_{t+1}^a = \mathbf{x}_{t+1}^f + \mathbf{K}_{t+1} [\mathbf{Y}_{t+1}^{obs} - \mathbf{H}_{t+1}(\mathbf{x}_{t+1}^f)], \quad (5)$$

$$\mathbf{K}_{t+1} = \mathbf{P}_{t+1}^f \mathbf{H}_{t+1}^T (\mathbf{H}_{t+1} \mathbf{P}_{t+1}^f \mathbf{H}_{t+1}^T + \mathbf{R}_{t+1})^{-1}, \quad (6)$$

$$\mathbf{x}_{i,t+1}^f = f(\mathbf{x}_{i,t}^a, \theta_{i,t+1}, \mathbf{u}_{i,t+1}) + \mathbf{w}, \mathbf{w} \sim N(0, \sigma_m), \quad (7)$$

$$\mathbf{x}_{i,t+1}^a = \mathbf{x}_{i,t+1}^f + \mathbf{K}_{t+1} [\mathbf{Y}_{t+1}^{obs} - \mathbf{H}_{t+1}(\mathbf{x}_{i,t+1}^f) + \mathbf{v}], \mathbf{v} \sim N(0, \sigma_o), \quad (8)$$

$$\bar{\mathbf{x}}_{t+1}^a = \frac{1}{N} \sum_{i=1}^N \mathbf{x}_{i,t+1}^a, \quad (9)$$

where f is the hydrodynamic model; \mathbf{x}_{t+1}^f and \mathbf{x}_t^a are, respectively, the states (water stages and discharges) of the hydrodynamic model at $t + 1$ and t time steps; θ_{t+1} and \mathbf{u}_{t+1} are, respectively, the model parameter (Manning's roughness coefficient) and forcing data (inflow boundary conditions) at $t + 1$ time step; \mathbf{K}_{t+1} and \mathbf{H}_{t+1} are, respectively, the Kalman gain matrix and the observation operator; \mathbf{Y}_{t+1}^{obs} is the observed state at $t + 1$ time step; \mathbf{P}_{t+1}^f is the model state error covariance matrix; \mathbf{R}_{t+1} is the observation noise covariance; $\mathbf{x}_{i,t+1}^f$ and $\mathbf{x}_{i,t}^a$ are, respectively, the states (water stages and discharges) of the i th ensemble member at $t + 1$ and t time steps; $\theta_{i,t+1}$ and $\mathbf{u}_{i,t+1}$ are, respectively, the ensemble member parameter (Manning's roughness coefficient) and forcing data (inflow boundary conditions) at $t + 1$ time step; \mathbf{w} is the model error with a mean of zero and standard deviation σ_m ; \mathbf{v} is the observation error with a mean of zero and standard deviation σ_o ; $\bar{\mathbf{x}}_{t+1}^a$ is the mean of ensemble members; and N is the number of ensemble members. The EnKF has been widely applied in hydrodynamic modeling. In the EnKF, it is assumed that \mathbf{x}_{t+1}^f follows a Gaussian distribution so that the posterior states are only determined by the first two moments (the mean and the covariance) of the prior density (Xu et al., 2017). However, the assumption is generally invalid in nonlinear hydrodynamic models (Pasetto et al., 2012).

The PF is a sequential data assimilation method utilizing Monte Carlo ensemble filter methods (Moradkhani, Hsu, et al., 2005). Compared to the widely used EnKF, the PF can relax the assumption of

the EnKF that the prior distributions of model states are Gaussian distributions (K. Kim et al., 2014; J. C. Neal et al., 2007) and is suitable for nonlinear and non-Gaussian hydrodynamic models and water environment models (Mattern et al., 2013; Xu et al., 2017). For the nonlinear and non-Gaussian HydroM2D model, its recursive formulation of model states can be expressed as

$$\mathbf{x}_{t+1} = f(\mathbf{x}_t, \theta_{t+1}, \mathbf{u}_{t+1}) + \mathbf{v}_{t+1}, \mathbf{v}_{t+1} \sim N(0, \sigma_m), \quad (10)$$

where f is the HydroM2D model; \mathbf{x}_{t+1} and \mathbf{x}_t are, respectively, the model states (water stages and discharges) at $t + 1$ and t time steps; θ_{t+1} and \mathbf{u}_{t+1} are, respectively, the model parameter (Manning's roughness coefficient) and forcing data (inflow boundary conditions) at $t + 1$ time step; and \mathbf{v}_{t+1} is the random white noise associated with the uncertainty of the HydroM2D model structure at $t + 1$ time step with a mean of zero and standard deviation σ_m .

The physical significance of equation (10) is to realize the recursive estimation of model states \mathbf{x} from t to $t + 1$ time step with the HydroM2D model and obtain the prior distribution $p(\mathbf{x}_{t+1}|\mathbf{x}_t)$ of model states \mathbf{x}_{t+1} at $t + 1$ time step. Assuming that the model states at $t + 1$ and previous time steps are observed as $\mathbf{y}_{1:t+1} = [y_1, y_2, \dots, y_t, y_{t+1}]$ and observations $\mathbf{y}_{1:t+1}$ are independent, according to the Bayesian theory (equation (11)), the posterior distribution $p(\mathbf{x}_{t+1}|\mathbf{y}_{1:t+1})$ of model states \mathbf{x}_{t+1} at $t + 1$ time step can be calculated with equation (12):

$$p(b|a) = \frac{p(a|b)}{p(a)}p(b), \quad (11)$$

$$p(\mathbf{x}_{t+1}|\mathbf{y}_{1:t+1}) = \frac{p(\mathbf{y}_{1:t+1}|\mathbf{x}_{t+1})p(\mathbf{x}_{t+1})}{p(\mathbf{y}_{1:t+1})} = \frac{p(\mathbf{y}_{t+1}, \mathbf{y}_{1:t}|\mathbf{x}_{t+1})p(\mathbf{x}_{t+1})}{p(\mathbf{y}_{t+1}, \mathbf{y}_{1:t})}. \quad (12)$$

According to the condition probability definition, $p(\mathbf{y}_{t+1}, \mathbf{y}_1 : t)$ can be expressed as

$$p(\mathbf{y}_{t+1}, \mathbf{y}_{1:t}) = p(\mathbf{y}_{t+1}|\mathbf{y}_{1:t})p(\mathbf{y}_{1:t}). \quad (13)$$

According to the joint distribution probability equation, $p(\mathbf{y}_{t+1}, \mathbf{y}_1 : t|\mathbf{x}_{t+1})$ can be expressed as:

$$p(\mathbf{y}_{t+1}, \mathbf{y}_{1:t}|\mathbf{x}_{t+1}) = p(\mathbf{y}_{t+1}|\mathbf{y}_{1:t}, \mathbf{x}_{t+1})p(\mathbf{y}_{1:t}|\mathbf{x}_{t+1}). \quad (14)$$

According to the Bayesian theory, $p(\mathbf{y}_1 : t|\mathbf{x}_{t+1})$ can be expressed as

$$p(\mathbf{y}_{1:t}|\mathbf{x}_{t+1}) = \frac{p(\mathbf{x}_{t+1}|\mathbf{y}_{1:t})p(\mathbf{y}_{1:t})}{p(\mathbf{x}_{t+1})}. \quad (15)$$

Substituting equations (13)–(15) into equation (12), $p(\mathbf{x}_{t+1}|\mathbf{y}_1 : t+1)$ can be expressed as

$$p(\mathbf{x}_{t+1}|\mathbf{y}_{1:t+1}) = \frac{p(\mathbf{y}_{t+1}|\mathbf{y}_{1:t}, \mathbf{x}_{t+1})p(\mathbf{x}_{t+1}|\mathbf{y}_{1:t})}{p(\mathbf{y}_{t+1}|\mathbf{y}_{1:t})}. \quad (16)$$

Assume that the observations are independent, $p(\mathbf{y}_{t+1}|\mathbf{y}_1 : t, \mathbf{x}_{t+1})$ can be expressed as

$$p(\mathbf{y}_{t+1}|\mathbf{y}_{1:t}, \mathbf{x}_{t+1}) = p(\mathbf{y}_{t+1}|\mathbf{x}_{t+1}). \quad (17)$$

Substituting equation (17) into equation (16), $p(\mathbf{x}_{t+1}|\mathbf{y}_1 : t+1)$ can be expressed as

$$p(\mathbf{x}_{t+1}|\mathbf{y}_{1:t+1}) = \frac{p(\mathbf{y}_{t+1}|\mathbf{x}_{t+1})p(\mathbf{x}_{t+1}|\mathbf{y}_{1:t})}{p(\mathbf{y}_{t+1}|\mathbf{y}_{1:t})}. \quad (18)$$

It is difficult to calculate analytical solutions of equation (18) due to nonlinear and non-Gaussian characteristics of the HydroM2D model. The PF is often used to derive the posterior distributions of model states. The PF employs a set of particles with weights to estimate the posterior distributions of model states and can

approximately explore the true posterior distributions of model states when the number of particles tends to infinity. In practice, a limited number of particles can be used to approximate the posterior distribution due to computation resource limitation. Assuming that N particles $\{\mathbf{x}_{t+1}^i, w_{t+1}^i\}_{i=1}^N$ have been sampled from the posterior distribution $p(\mathbf{x}_{t+1}|y_{t+1})$, the posterior distribution $p(\mathbf{x}_{t+1}|y_{t+1})$ can be approximately calculated as

$$p(\mathbf{x}_{t+1}|y_{t+1}) \approx w_{t+1}^i \sum_{i=1}^N \delta(\mathbf{x}_{t+1} - \mathbf{x}_{t+1}^i), \quad (19)$$

where δ is the Dirac delta function and w_{t+1}^i is the weight of the i th particle \mathbf{x}_{t+1}^i at $t + 1$ time step.

The PF has many procedures for weight updating (Moradkhani, Hsu, et al., 2005; Van Leeuwen, 2009). Sampling Importance Resampling was adopted to update the particle weight w_{t+1}^i (equation (20)):

$$w_{t+1}^i = \frac{w_t^i p(y_{t+1}|\mathbf{x}_{t+1}^i)}{\sum_{i=1}^N w_t^i p(y_{t+1}|\mathbf{x}_{t+1}^i)}, \quad (20)$$

where $p(y_{t+1}|\mathbf{x}_{t+1}^i)$ is the likelihood between y_{t+1} and \mathbf{x}_{t+1}^i .

Finally, the optimal estimations of the HydroM2D model states can be derived from the posterior distributions of the HydroM2D model states by means of weighted average method:

$$\hat{\mathbf{x}}_{t+1} = \sum_{i=1}^N w_{t+1}^i \mathbf{x}_{t+1}^i. \quad (21)$$

In the PF, particle weight update unavoidably leads to particle degeneracy (Snyder et al., 2008). In the particle degeneracy phenomenon, only a few particles have greater weights and the weights of remaining particles tend to zero. Particle degeneracy will consume too much computing resource to update the particles with weights approximating to zero. Resampling is a most commonly used method to solve this problem and it replicates the particles with greater weights and deletes the particles with small weights. Here the multinomial resampling method proposed by Gordon et al. (1993) was adopted. First, N random numbers (r_k) are generated from uniform distribution $U(0,1]$. Second, the cumulative weight sequence is calculated as follows: $c^i = c^{i-1} + w_{t+1}^i, c^0 = 0$. Third, the number N^i of r_k which belongs to the interval $(c^{i-1}, c^i], i = 1, 2, \dots, N$ is counted. Finally, the i th particle \mathbf{x}_{t+1}^i is duplicated for N^i times. After duplication for N times, the same weight $1/N$ is assigned to all the particles.

Resampling for solving particle degeneracy may result in “sample impoverishment”. Sample impoverishment refers to the case that the diversity of particles may deteriorate due to many times of duplications of some particles with large weights in resample. Therefore, in order to maintain the particle diversity, a kernel smoothing method (Moradkhani et al., 2005; Qin et al., 2009; West, 1993) is used to perturb Manning’s roughness coefficients of particles after resampling. The kernel smoothing method can be expressed as

$$p(\theta_{t+1}|\theta_t) \sim N\left(\theta_{t+1}^i | \sqrt{1-h^2}\theta_t^i + (1-\sqrt{1-h^2})\bar{\theta}_t, h^2 V_t\right), \quad (22)$$

where θ_{t+1} and θ_t are the Manning’s roughness coefficients of particles at $t + 1$ and t time steps, respectively; θ_{t+1}^i and θ_t^i are the Manning’s roughness coefficients of the i th particle at $t + 1$ and t time steps, respectively; $\bar{\theta}_t$ is the mean of Manning’s roughness coefficients of particles at t time step; h is the smoothing parameter for controlling the degree of the perturbation of Manning’s roughness coefficient, which increases with the increase in h ; and V_k is the variance of Manning’s roughness coefficients of particles at t time step. Compared to random perturbation, the kernel smoothing method can avoid the gradual increase in the variance of Manning’s roughness coefficients (Qin et al., 2009).

In the MPFDA-LW for the HydroM2D model, the computational domain is discretized by structured grids. Each grid cell has its own particle set which involves model states (water stage, discharge) and the model parameter (Manning’s roughness coefficient). Particles in different computational grid cells have different weights (local weighting procedure) and Manning’s roughness coefficients (spatial variability of

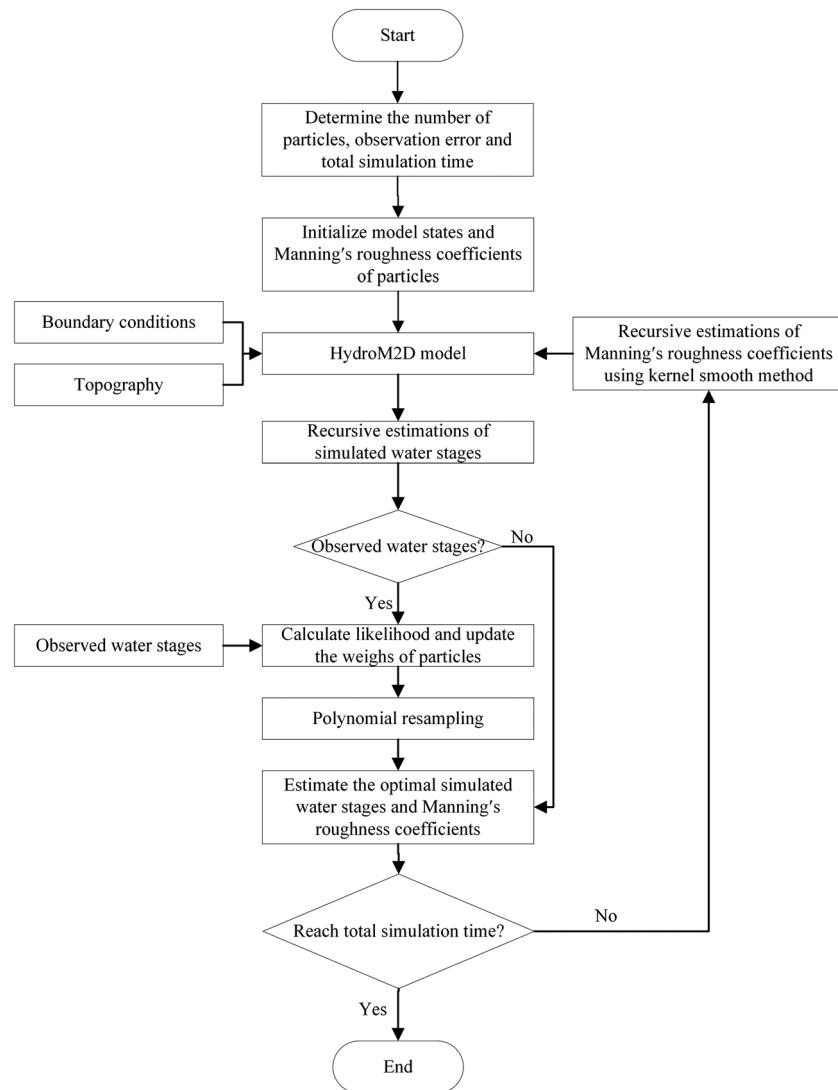


Figure 1. Framework of the MPFDA-LW for the HydroM2D model considering the spatial-temporal variability of Manning's roughness coefficient.

Manning's roughness coefficient). Observed water stages are assimilated into the HydroM2D model to simultaneously update simulated water stages and discharges as well as Manning's roughness coefficients (temporal variability of Manning's roughness coefficient). The framework of the MPFDA-LW for the HydroM2D model considering spatial-temporal variability of Manning's roughness coefficient is shown in Figure 1. The detailed procedures of the MPFDA-LW for the HydroM2D model are described as follow:

Step 1. N particles (equations (23)–(27)) are generated for N_c computational grid cells at the initial time step (t), respectively. The N particles (\mathbf{P}) of N_c computational grid cells jointly represent N flow states. The water stage, discharge, and Manning's roughness coefficient of each particle are, respectively, generated by adding noises extracted from uniform distributions. To achieve the wider prior distributions of water stages of particles in the next time step ($t + 1$), N Manning's roughness coefficients of particles at each computational grid cell are sorted in the descending order. The weight of each particle is set as $1/N$.

$$\mathbf{P}_t^{i,j} = [\mathbf{x}_t^{i,j}, n_t^{i,j}], \mathbf{x}_t^{i,j} = [z_t^{i,j}, Q_t^{i,j}], i = 1, 2, \dots, N; j = 1, 2, \dots, N_c, \quad (23)$$

$$z_t^{i,j} = z_t^j + \varepsilon_z^j, \varepsilon_z^j \sim U(-0.01z_t^j, 0.01z_t^j), \quad (24)$$

$$Q_t^{i,j} = Q_t^j + \varepsilon_Q^j, \varepsilon_Q^j \sim U(-0.1Q_t^j, 0.1Q_t^j), \quad (25)$$

$$\begin{aligned} n_t^{i,j} &= n_t^j + \varepsilon_n^j, \varepsilon_n^j \sim U(-0.01, 0.01), \\ n_t^{i,j} &\geq n_t^{i+1,j}, i = 1, 2, \dots, N-1, j = 1, 2, \dots, N_c \end{aligned} \quad (26)$$

$$w_t^{i,j} = 1/N, i = 1, 2, \dots, N; j = 1, 2, \dots, N_c, \quad (27)$$

where $z_t^{i,j}$ and $Q_t^{i,j}$ are, respectively, the simulated water stages and discharges of the i th particle at the j th computational grid cell ($\mathbf{P}_t^{i,j}$); z_t^j and Q_t^j are, respectively, the simulated water stages and discharges of the model; $n_t^{i,j}$ and n_t^j are, respectively, the Manning's roughness coefficient of the i th particle and the initial Manning's roughness coefficient at the j th computational grid cell; ε_z^j , ε_Q^j , and ε_n^j are, respectively, the perturbation errors of simulated water stages and discharges as well as Manning's roughness coefficient at the j th computational grid cell; $w_t^{i,j}$ is the weight of the i th particle at the j th computational grid cell; and U refers to a uniform distribution.

Step 2. N sets of inflow boundary condition ($\mathbf{Q}_{\text{inflow}}^{i,t+1}$) at $t + 1$ time step are generated by adding noises extracted from Gaussian distributions (equation (28)):

$$\mathbf{Q}_{\text{inflow}}^{i,t+1} = \mathbf{Q}_{\text{inflow}}^{\text{obs},t+1} + N(0, 0.01\mathbf{Q}_{\text{inflow}}^{\text{obs},t+1}), \quad (28)$$

where $\mathbf{Q}_{\text{inflow}}^{\text{obs},t+1}$ is the observed inflow discharge at $t + 1$ time step.

Step 3. Perturb Manning's roughness coefficients of particles at the computational grid cells with gauges.

$$p(n_{t+1}^{i,j} | n_t^{i,j}) \sim N(n_{t+1}^{i,j} | \sqrt{1-h^2}n_t^{i,j} + (1-\sqrt{1-h^2})\bar{n}_t^j, h^2V_t), i = 1, 2, \dots, N; j = k_1, k_2, \dots, k_m, \quad (29)$$

where \bar{n}_t^j is the mean of Manning's roughness coefficients of particles at the j th computational grid cell and k_m is the number of the computational grid cells with gauges.

Step 4. Drive the HydroM2D model by \mathbf{x}_t^i , n_{t+1}^i , and $\mathbf{Q}_{\text{inflow}}^{i,t+1}$ and simulate the water stage and discharge with equation (30) at each computational grid cell at the next time step (\mathbf{x}_{t+1}^i). Note that the white noise associated with the model structure is not considered.

$$\mathbf{x}_{t+1}^i = f(\mathbf{x}_t^i, n_{t+1}^i, \mathbf{Q}_{\text{inflow}}^{i,t+1}). \quad (30)$$

Step 5. Calculate likelihoods of particles and update the weights of particles. If there are N_{obs} observed water stages $z_{\text{obs},t+1}^j, j = 1, 2, \dots, N_{\text{obs}}$ at N_{obs} computational grid cells at $t + 1$ time step, the weight of the i th particle is calculated with equation (31). Otherwise, skip to step 7.

$$w_{t+1}^{i,j} = p(z_{\text{obs},t+1}^j | z_{t+1}^{i,j}) = \frac{1}{\sqrt{2\pi\sigma_{\text{obs}}}} \exp\left(-\frac{(z_{\text{obs},t+1}^j - z_{t+1}^{i,j})^2}{2\sigma_{\text{obs}}^2}\right), \quad (31)$$

where σ_{obs} is the observed standard deviation.

Step 6. Resample the particles at the gauges with observations according to the multinomial resample method based on the weights of particles. The new particles will have the same weights.

Step 7. Estimate optimal model states and Manning's roughness coefficient at each gauge at $t + 1$ time step with equations (32) and (33):

$$\hat{\mathbf{x}}_{t+1}^j = \sum_i w_{t+1}^{i,j} \mathbf{x}_{t+1}^i, \quad (32)$$

$$\hat{n}_{t+1}^j = \sum_{i=1}^N w_{t+1}^{i,j} n_{t+1}^{i,j}. \quad (33)$$

Step 8. Let $t = t + 1$, repeat steps 3–7 until t is equal to total simulation time.

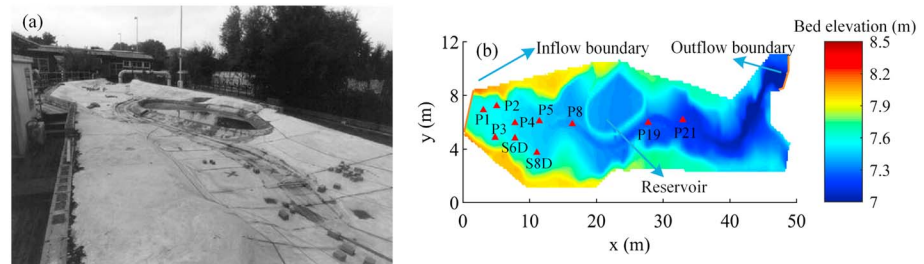


Figure 2. (a) General view of Toce River physical model and (b) its topography as well as the locations of gauges.

Compared to the MPFDA-LW, the PFDA-GW adopts spatially uniform Manning's roughness coefficients. Each particle represents a flow state (e.g., water stages and discharges) and Manning's roughness coefficients (uniform value) at all computational grid cells. The weight of certain particle is calculated with the sub-weights of the particle at the computational grid cells with gauges according to the joint probability theory (Giustarini et al., 2011; Xu et al., 2017). The optimal model states and Manning's roughness coefficients at all computational grid cells at $t + 1$ time step are estimated with equations (34) and (35). The details of the PFDA-GW can be found in the report by Giustarini et al. (2011).

$$\hat{\mathbf{x}}_{t+1}^j = \sum_{i=1}^N w_{t+1}^i \mathbf{x}_{t+1}^{i,j}, \quad (34)$$

$$\hat{n}_{t+1} = \sum_{i=1}^N w_{t+1}^i n_{t+1}^i, \quad (35)$$

where w_{t+1}^i is the global weight of the i th particle at $t + 1$ time step and \hat{n}_{t+1} is the optimal Manning's roughness coefficient of the HydroM2D model at $t + 1$ time step.

2.3. Physical Model of Toce River

A physical model (Figure 2a) was established by Ente Nazionale per L'energia Elettrica according to a scale of 1:100 in the 5 km upstream of Toce River in Milan, Italy (Soares Frazão, 1999). The physical model of Toce River is a standard model and widely used to test the accuracy and stability of various hydrodynamic models in simulating dam-break flood (Lai & Khan, 2012; D. F. Liang et al., 2007; Prestininzi, 2008). It is about 50 m long and 11 m wide. A DEM with a spatial resolution of 5 cm was used to accurately describe the topography (Figure 2b). There was a reservoir with an opening at the river side. The opening was always closed during the experiments. Several gauges scattered over the entire model were used to record the time evolution of water depth (observation frequency of 1 s), but the discharge was not measured. We only obtained the water stages at 10 gauges shown in Figure 2b. Inflow boundary conditions of this physical model (Figure 2b) were realized by suddenly increasing the water level in a tank. The inflow discharge process within 180 s (observation frequency of 1 s) is shown in Figure 3. A free outflow (Figure 2b) was set in the hydrodynamic model. In the physical model, the initial water depth was 0 m.

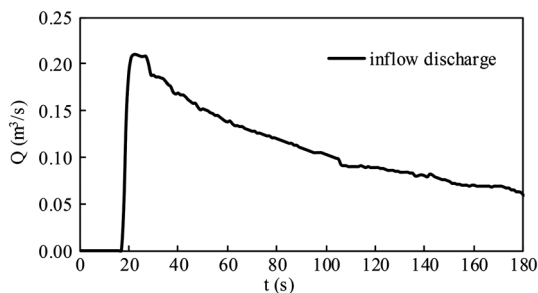


Figure 3. Inflow discharge hydrograph.

In this study, we adopted the physical model of Toce River to validate the performance of the MPFDA-LW for the HydroM2D model. The Manning's roughness coefficient was recommended to be $0.0162 \text{ s/m}^{1/3}$ by Ente Nazionale per L'energia Elettrica. The computational domain was discretized into structural grid cells with a grid cell size of 0.1 m. The DEM of grid cell center was interpolated based on the DEM with a spatial resolution of 5 cm. The grid cell size of 2-D hydrodynamic models for a specific scenario depended on the geography and observation conditions. If 2-D hydrodynamic models were used to simulate the flow on flat basins or the basins with low-resolution DEM observation, the grid cell size would be increased.

2.4. PF-Based Data Assimilation Evaluation

The performances of the MPFDA-LW, the PFDA-GW, and the open-loop HydroM2D model were evaluated in terms of root-mean-square errors (RMSE), average relative error (ARE), and Kling-Gupta efficiency (KGE; Gupta et al., 2009). RMSE and ARE, respectively, refer to the absolute and relative errors between simulated and observed values. KGE is a comprehensive criterion for evaluating the consistency between simulated and observed values based on correlation (r), variability error (α), and bias error (β). RMSE, ARE, and KGE are expressed as

$$\text{RMSE} = \sqrt{\frac{\sum_{i=1}^T (z_i - z_{\text{obs}})^2}{T}}, \quad (36)$$

$$\text{ARE} = \frac{\sum_{i=1}^T |z_i - z_{\text{obs}}| / z_{\text{obs}}}{T}, \quad (37)$$

$$\text{KGE} = 1 - \sqrt{(r-1)^2 + (\alpha-1)^2 + (\beta-1)^2}, \quad (38)$$

$$\alpha = \sigma_s / \sigma_o, \quad (39)$$

$$\beta = \mu_s / \mu_o, \quad (40)$$

where z_i is the assimilated/simulated water stages at the i th second; z_{obs}^i is the observed water stages in the i th second; T is the total assimilation time; r is the correlation coefficient between assimilated/simulated water stages and observed water stages; α is a measure of relative variability in the simulated and observed values; σ_s and σ_o are the standard deviations of assimilated/simulated and observed water stages, respectively; β is the bias error; and μ_s and μ_o are the means of assimilated/simulated and observed water stages.

3. Results and Discussion

3.1. Performance of the HydroM2D Model

Water stages at 10 gauges were simulated with the HydroM2D model within 180 s. The mean RMSE, ARE, and KGE of simulated water stages against observed water stages at the 10 gauges were 0.011 m, 0.11%, and 0.83, respectively. Simulated water stages at gauges P1, P2, P8, P19, P21, and S6D are shown in Figure 4. Simulated water stages at gauges P19 and P21 were consistent with observations, but the HydroM2D model overestimated or underestimated the water stages at the other four gauges. The model cannot exactly predict the water stages due to the potential errors of model structures, topography, and grid discretization (D. F. Liang, Lin, & Falconer, 2007; Prestininzi, 2008). In addition, Manning's roughness coefficient is a spatial-temporal parameter associated with riverbed roughness and flow conditions (Y. Kim et al., 2013; Xu et al., 2017). The HydroM2D model adopts a constant Manning's roughness coefficient, so it is difficult to exactly predict the observed water stages at each gauge with the model.

3.2. Sensitivity Analysis of PF-Based Data Assimilation Parameters

The number of particles (N), observation error (σ_o), and assimilation frequency (AF) have significant influences on the performance of PF-based data assimilation (Matgen et al., 2010; Plaza et al., 2012; H. J. Zhang et al., 2013). In order to determine the three parameters, we analyzed the sensitivities of the three parameters of the MPFDA-LW to the HydroM2D model in simulating dam-break flood inundation based on the physical model of Toce River. In the sensitivity analysis, the ranges, step sizes, and initial values of N , σ_o , and AF are provided in Table 1. The sensitivity of a certain parameter was analyzed with the initial values of the other two parameters.

Observed water stages within 180 s at the 10 gauges were assimilated in the MPFDA-LW for the HydroM2D model. The mean KGE of assimilated water stages derived from the PF-based data assimilation against observed water stages at the 10 gauges with the increase in the N , σ_o , and AF are shown in Figure 5. The mean KGE of assimilated water stages at the 10 gauges marginally increased with the increase in N as a

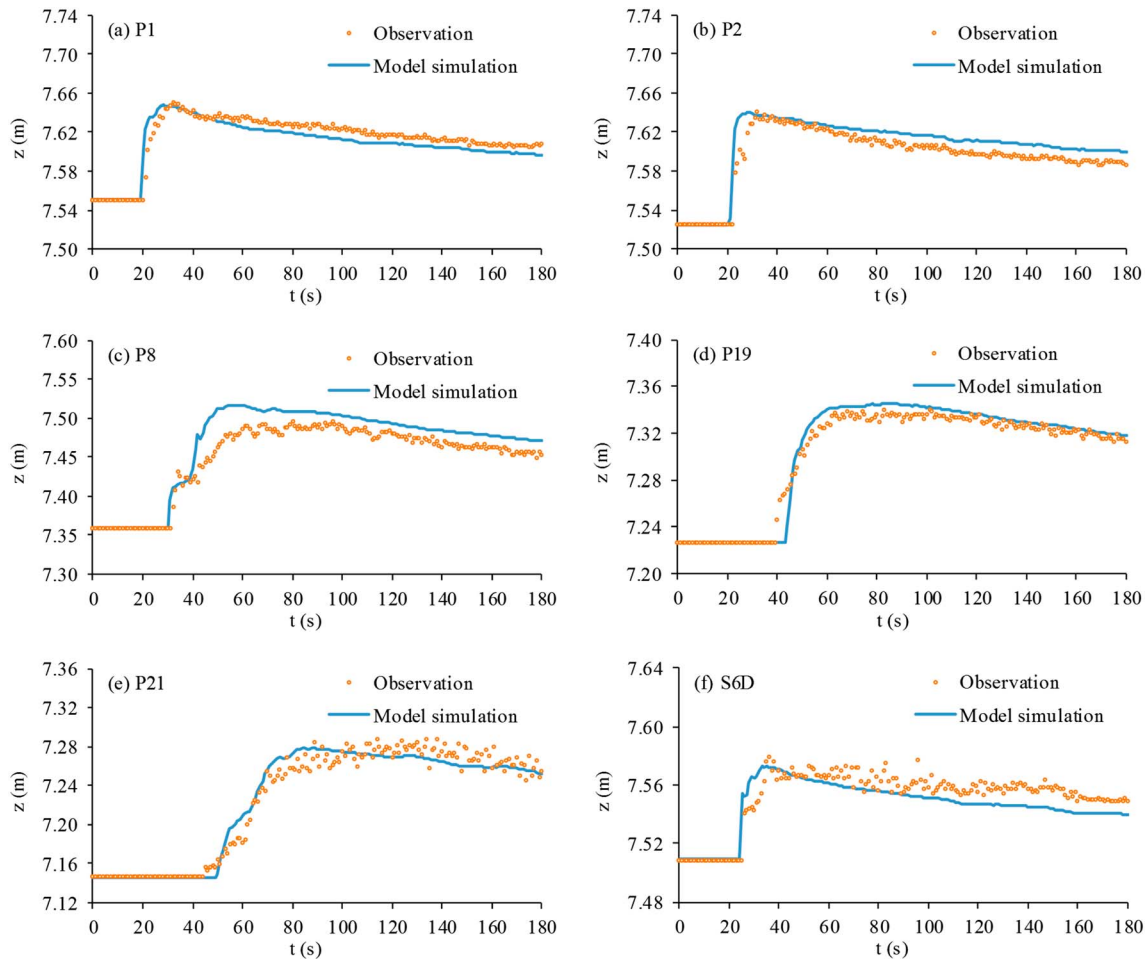


Figure 4. Water stages at gauges (a) P1, (b) P2, (c) P8, (d) P19, (e) P21, and (f) S6D simulated with the HydroM2D model and observations. Blue full lines and red circles, respectively, refer to open-loop assimilations and observations of water stages.

whole. However, runtime of the PF-based data assimilation linearly increased with the increase in N (Figure 5a; H. J. Zhang et al., 2013). Therefore, N was set to be 100 in order to simultaneously obtain the high computational efficiency and assimilation accuracy of the PF-based data assimilation. The mean KGE of assimilated water stages at the 10 gauges increased with the increase in σ_o and AF (Figures 5b and 5c; Matgen et al., 2010; Plaza et al., 2012). Therefore, σ_o and AF were, respectively, set to be 0.01 m and 1 s.

In general, the assimilation accuracy increases with the increase in the number of particles, but runtime proportionally increases with the increase in the number of particles (Han & Li, 2008). The performance of PF-based data assimilation is sensitive to the standard deviation of observation errors (Han & Li, 2008). A small standard deviation of observation error will result in the serious degeneracy phenomenon in the PF-based data assimilation (Han & Li, 2008), whereas a large standard deviation of observations will result

in the small sensitivity of particle weights to observations and decrease the performance of PF-based data assimilation (Matgen et al., 2010). In addition, the PF-based data assimilation with a high assimilation frequency can avoid error accumulation and improve its performance through the timely assimilation of observations at more time steps (Plaza et al., 2012). In practice, the three parameters of the PF-based data assimilation for hydrodynamic models for a specific scenario should be determined according to application requirements and observation conditions.

Table 1
Ranges, Step Sizes, and Initial Values of N , σ_o , and AF

Parameters	Initial value	Minimum	Maximum	Step
N	100	20	200	20
σ_o	0.01	0.01	0.05	0.01
AF	1	1	8	1

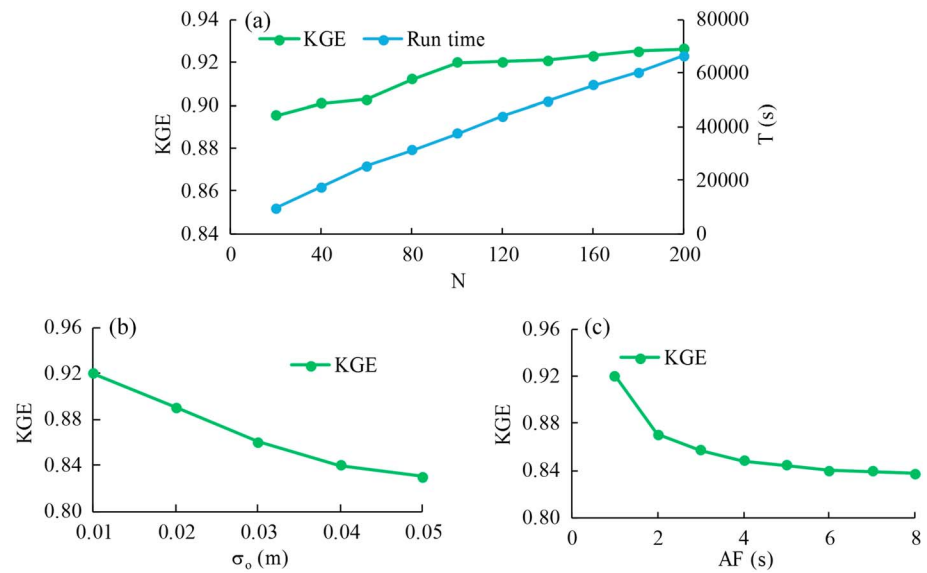


Figure 5. Mean KGE of assimilated water stages at the 10 gauges derived from the MPFDA-LW for the HydroM2D model with (a) different numbers of particles, (b) observation errors, and (c) assimilation frequencies, as well as runtime of MPFDA-LW with different numbers of particles (a).

3.3. Performances of the MPFDA-LW for the HydroM2D Model

In MPFDA-LW, the number of particles (N), observation error (σ_o), and assimilation frequency (AF) were, respectively, set as 100, 0.01 m, and 1 s. In the kernel smoothing method, h and V_k were, respectively, set as 0.2 and 3×10^{-4} . We assimilated the observed water stages from the 20th to 160th second (assimilation period) at the 10 gauges and used those of the 161th to 180th second to validate the propagation of assimilation effect in time dimension. Although we only assimilated the observed water stages into the HydroM2D model, the discharges and Manning's roughness coefficients coupled with water stages as a part of the particles were also corrected indirectly (Xu et al., 2017). The assimilated discharges were not analyzed in our study due to the lack of observed discharges. In addition, the assimilated surface water extents were not evaluated due to the lack of observed surface water extents.

Scatterplots of assimilated, simulated, and observed water stages at gauges P1, P2, P8, P19, P21, and S6D are shown in Figure 6. The points of assimilated water stages were closer to the 1:1 line than those of simulated water stages. The performance of the MPFDA-LW for the HydroM2D model (RMSE: 0.005 m, ARE: 0.05%, KGE: 0.91) was better than that of the open-loop simulation (RMSE: 0.011 m, ARE: 0.11%, KGE: 0.83).

The 90% confidence intervals of assimilated water stages at the 10 gauges are shown in Figure 7. These confidence intervals could not fully cover the observed water stages because only the uncertainty associated with Manning's roughness coefficient and inflow boundary conditions were considered in the MPFDA-LW for the HydroM2D model. In order to improve the performance of the MPFDA-LW for the HydroM2D model, other uncertainties associated with input data (e.g., river-bed geometry) and model structures (e.g., governing equations and numerical computation method) should be considered in the PF-based data assimilation coupled with the uncertainties associated with Manning's roughness coefficient and boundary conditions (Xu et al., 2017).

The MPFDA-LW for the HydroM2D model had good performances in the assimilation (the 20th to 160th second) and prediction periods (from the 161th to 180th second). In the assimilation period, the assimilations of water stages at different gauges derived from the MPFDA-LW were consistent with the observed water stages (Figure 7). In the prediction period, the assimilated water stages at different gauges were still close to the observed water stages, indicating that the assimilation effect of the MPFDA-LW for the HydroM2D model could propagate in the temporal dimension. Only the Manning's roughness coefficients at the 10 gauges were updated with the water stage assimilation, so the assimilation effects of the MPFDA-LW for the HydroM2D model could not propagate in the spatial dimension.

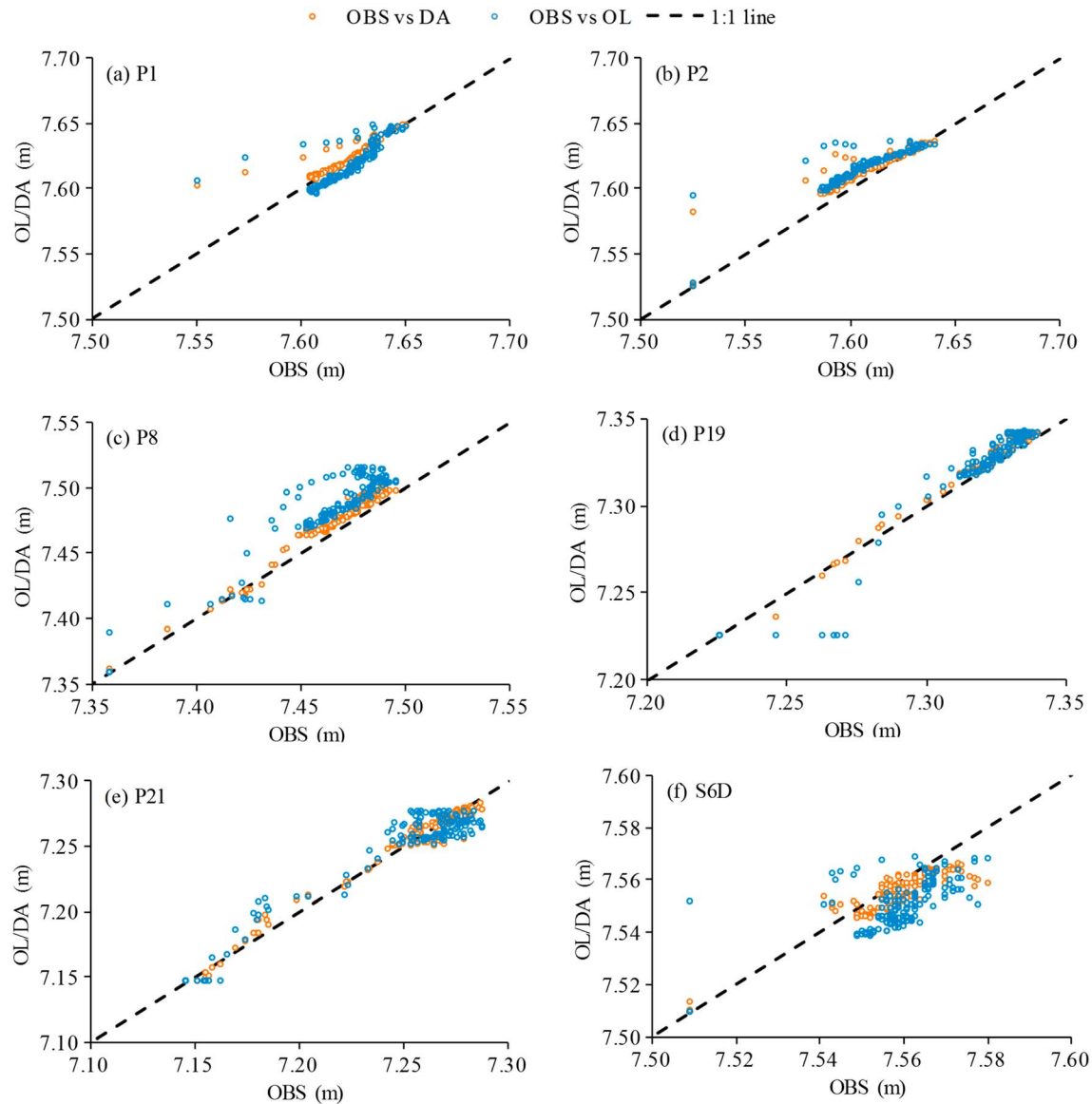


Figure 6. Scatterplots of assimilated (data assimilation (DA)), simulated (open loop (OL)), and observed (OBS) water stages at gauges P1, P2, P8, P19, P21, and S6D. Blue and red circles, respectively, indicate the points of “OBS versus OL” and “OBS versus DA.” Black line indicates the 1:1 line.

Figure 8 shows the optimal Manning’s roughness coefficients at the 10 gauges derived from the MPFDA-LW for the HydroM2D model. The optimal Manning’s roughness coefficients at different gauges gradually varied with time and showed the significant difference. It should be noted that the optimal Manning’s roughness coefficients derived from the MPFDA-LW for the HydroM2D model could not represent the true roughness because the weights of particles were calculated with the simulation errors of water stages, which included the uncertainties of river bed roughness, geography, inflow conditions, and other model errors (Camacho et al., 2015). The MPFDA-LW for the HydroM2D model could adaptively adjust Manning’s roughness coefficients according to particle weights. Consequently, the optimal Manning’s roughness coefficients derived from the MPFDA-LW for the HydroM2D model involved certain uncertainties associated with geography, inflow conditions, and other model errors.

The 90% confidence intervals of the Manning’s roughness coefficients at gauges P1, P2, P8, P19, P21, and S6D derived from the MPFDA-LW are shown in Figure 9. The 90% confidence intervals of Manning’s roughness coefficients at the six gauges varied with assimilation step and did not become narrow (Figure 9), indicating

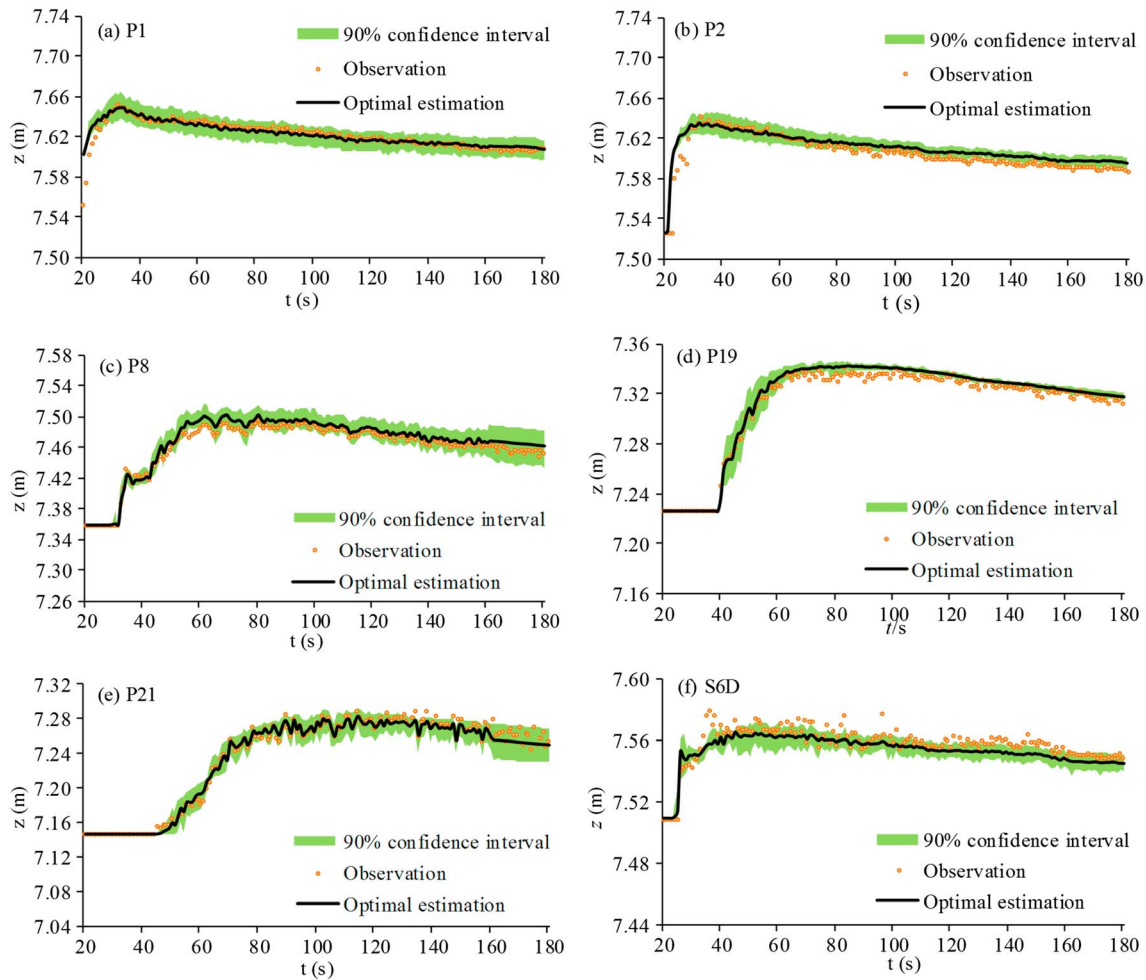


Figure 7. The 90% confidence intervals (green background) of assimilated water stages at gauges (a) P1, (b) P2, (c) P8, (d) P19, (e) P21, and (f) S6D derived from the MPFDA-LW for the HydroM2D model. Blue full lines, black full lines, and red circles, respectively, indicate the open-loop assimilations, assimilations, and observations of water stages.

that Manning's roughness coefficients had the significant uncertainty and obvious spatial-temporal variability. Figure 10 shows the spatial-temporal variability of Manning's roughness coefficients (e.g., the 20th second and 180th second). In the MPFDA-LW for the HydroM2D model, each grid cell had its own particle set and only the weights of the particles at the grid cells with gauges could be updated via water stage assimilation. The weights of the particles at other grid cells maintained their prior values ($1/N$).

Therefore, only the Manning's roughness coefficients at the 10 grid cells with gauges could be estimated with water stage assimilation and the Manning's roughness coefficients at other computational grid cells were prior values and fluctuated around the recommended value.

3.4. Performances of the PFDA-GW for the HydroM2D Model

The same parameters were set for the PFDA-GW for the HydroM2D model. Scatterplots of assimilated water stages at gauges P1, P2, P8, P19, P21, and S6D derived from the PFDA-GW are shown Figure 11. Only the points of assimilated water stages at gauges P1 and P2 were closer to the 1:1 line than those of simulated water stages. The performance of the PFDA-GW for the HydroM2D model (RMSE: 0.01 m, ARE: 0.10%, KGE: 0.85) was slightly better than that of the open-loop simulation (RMSE: 0.011 m, ARE: 0.11%, KGE: 0.83). In the PFDA-GW for

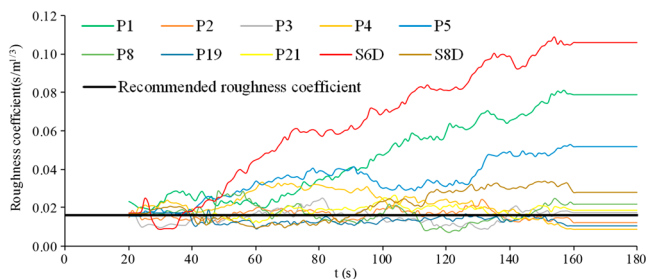


Figure 8. Optimal Manning's roughness coefficients at the 10 gauges derived from the MPFDA-LW for the HydroM2D model. Black line indicates the recommended Manning's roughness coefficient.

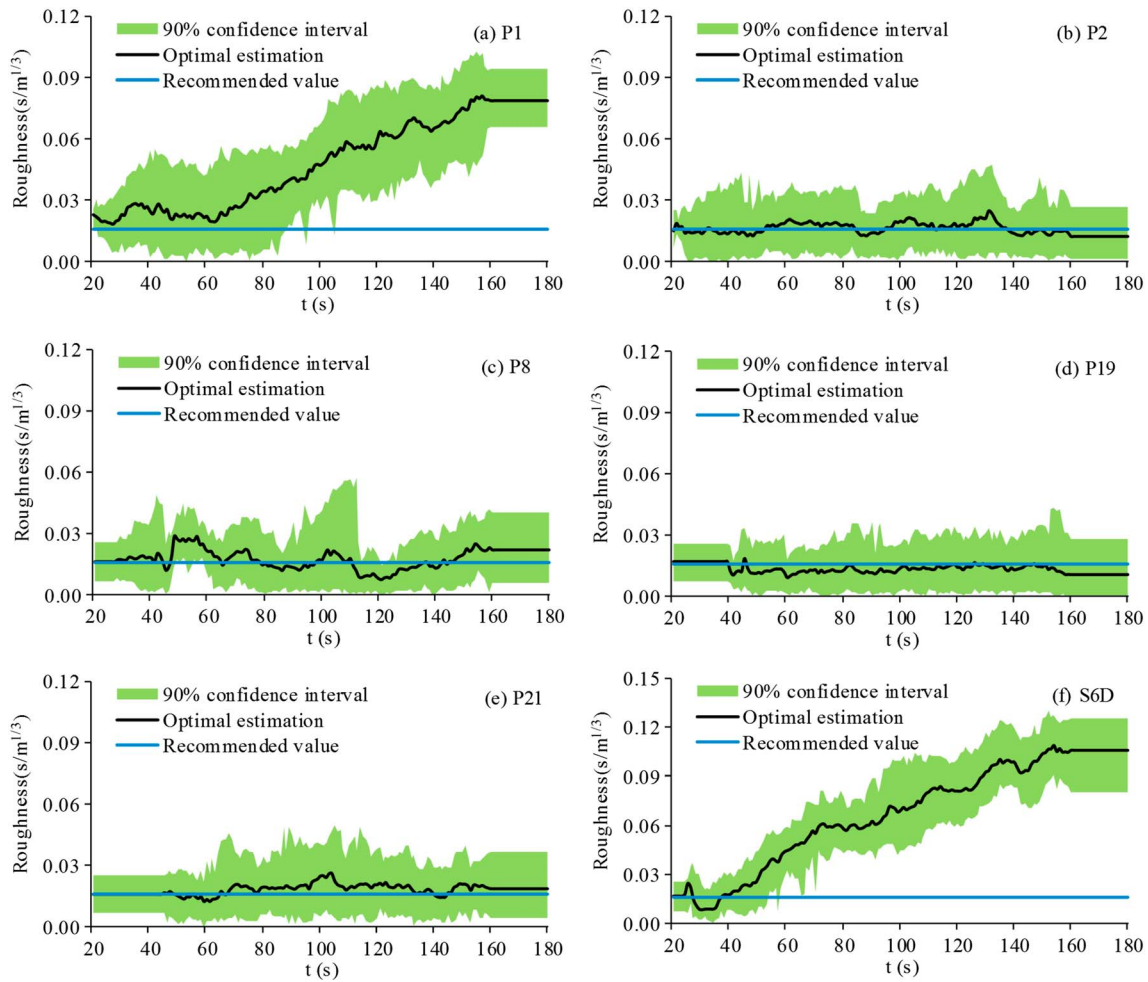


Figure 9. The 90% confidence intervals of the Manning's roughness coefficients at gauges (a) P1, (b) P2, (c) P8, (d) P19, (e) P21, and (f) S6D derived from the MPFDA-LW for the HydroM2D model.

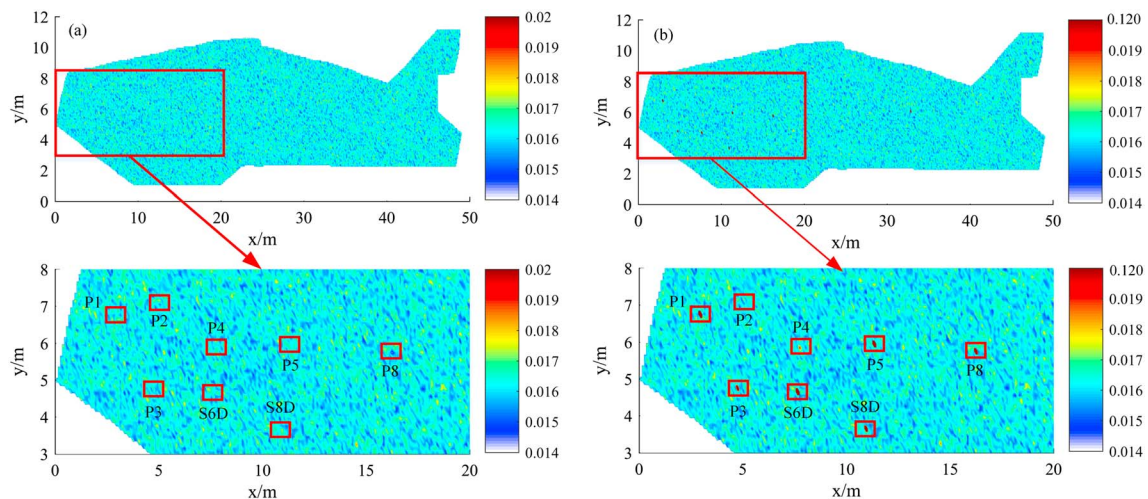


Figure 10. Spatial variability of Manning's roughness coefficients at the (a) 20th second and (b) 180th second.

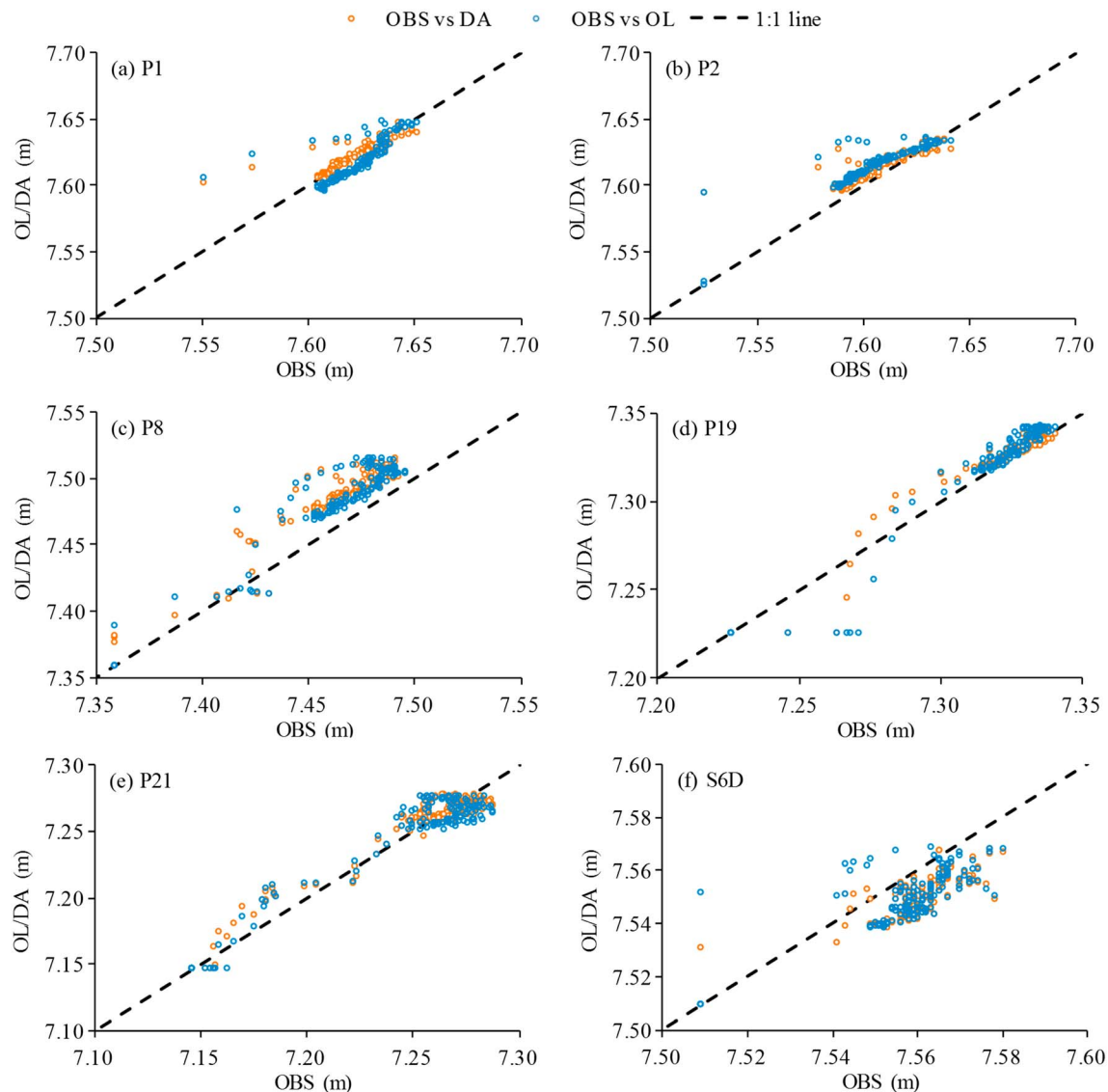


Figure 11. Scatterplots of the assimilated (data assimilation (DA)), simulated (open loop (OL)), and observed (OBS) water stages at gauges P1, P2, P8, P19, P21, and S6D. Blue and red circles, respectively, indicate the points of “OBS versus OL” and “OBS versus DA.” Black line indicates the 1:1 line.

HydroM2D model, particle weights simultaneously depended on the water stages of particles at all the 10 gauges. The PFDA-GW aims to obtain the global optimal estimation of water stages at all gauges. In addition, Manning’s roughness coefficient is a spatial-temporal parameter associated with riverbed roughness and flow conditions. The particles in the PFDA-GW for HydroM2D model with uniform Manning’s roughness coefficients cannot simultaneously obtain the optimal estimation at all the gauges due to potential errors of topography and spatial-temporal variability of Manning’s roughness coefficient (Giustarini et al., 2011; D. F. Liang, Lin, & Falconer, 2007; Prestininzi, 2008; Xu et al., 2017).

The characteristics of the 90% confidence intervals of assimilated water stages at different gauges derived from the PFDA-GW were different (Figure 12). The 90% confidence intervals of assimilated water stages at gauges P1, P2, and S6D near the inflow boundary were wider than those at gauges P5, P19, and P21 due to the perturbation influence of inflow discharge. The 90% confidence intervals of assimilated water stages at gauges P5, P8, P19, and P21 far away from the inflow boundary were extremely narrow. This phenomenon can be interpreted as follows. First, water stages of particles at gauges far away inflow boundary were less affected by the perturbation of inflow discharge. Second, the diversity of flow states of particles

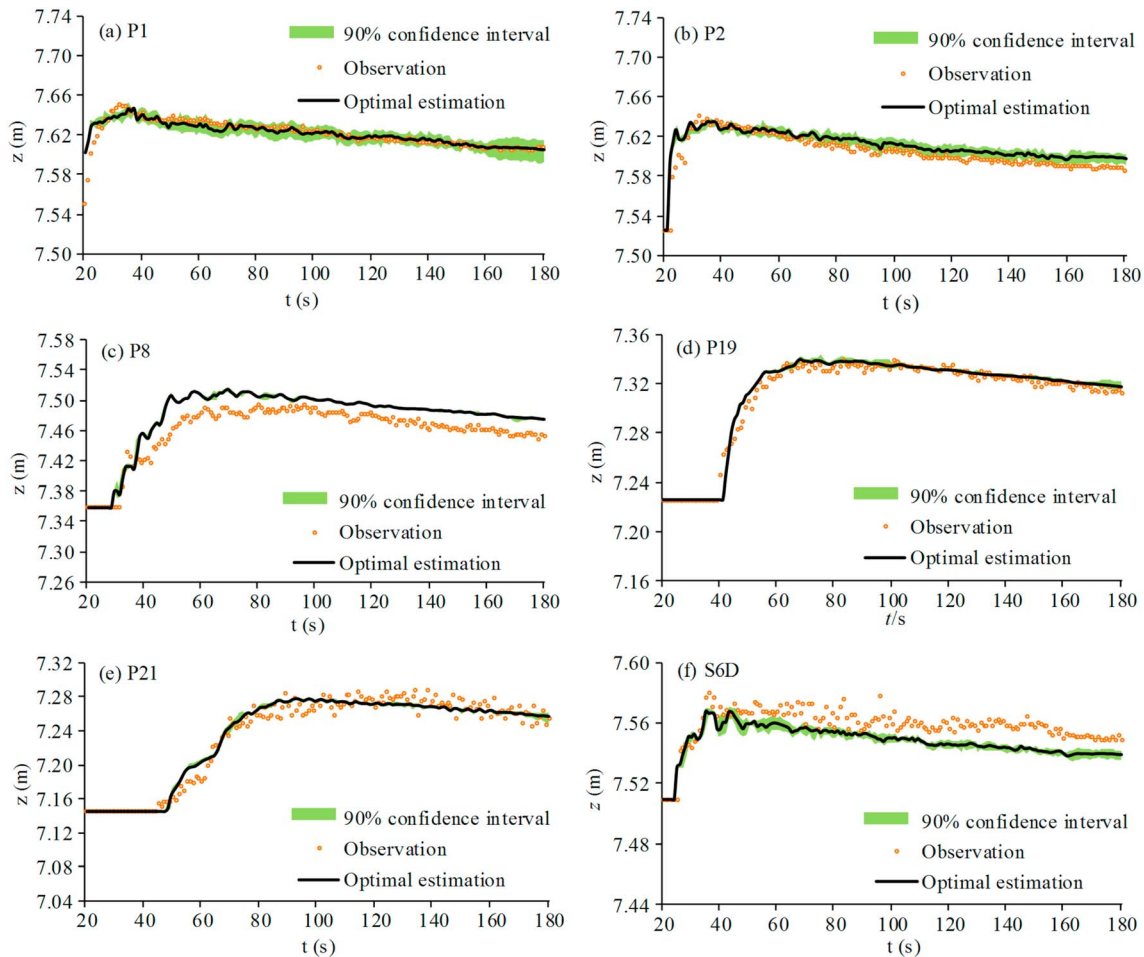


Figure 12. The 90% confidence intervals (green background) of assimilated water stages at gauges (a) P1, (b) P2, (c) P8, (d) P19, (e) P21, and (f) S6D derived from the PFDA-GW for the HydroM2D model. Blue full lines, black full lines, and red circles, respectively, indicate the open-loop assimilations, assimilations, and observations of water stages.

at a certain assimilation time step was significantly reduced after particle resampling through executing the perturbation of Manning's roughness coefficients (Y. Kim et al., 2013; Xu et al., 2017). Third, the high-frequency data assimilation (e.g., 1-s assimilation frequency) was adopted in simulating the dam-break

flood because it always drastically varied within a short period (Aureli et al., 2000). The three main factors in the PFDA-GW resulted in the narrow prior ranges of simulated water stages (gauge P21; Figure 13) and the narrow 90% confidence intervals. PFDA-GW had the poor ability to derive the prior range of simulated water stages.

The PFDA-GW for the HydroM2D model considering spatially uniform Manning's roughness coefficient could only estimate the temporal variability of Manning's roughness coefficients. The optimal estimation of Manning's roughness coefficient derived by the PFDA-GW for the HydroM2D model fluctuated around the recommended value (Figure 14). Particle weights in the PFDA-GW for the HydroM2D model simultaneously depended on simulated water stages at the 10 gauges, so the optimal estimation of Manning's roughness coefficients was the optimal global estimation of Manning's roughness coefficients at the 10 gauges.

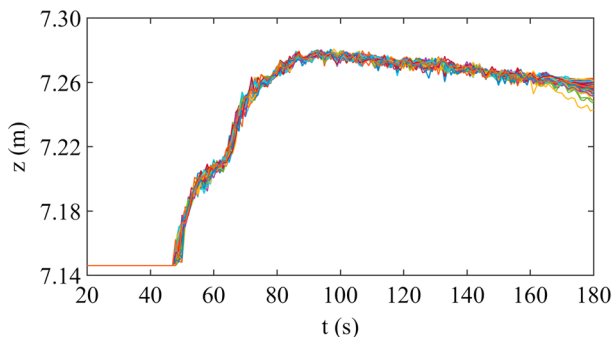


Figure 13. Prior ranges of simulated water stages of particles at gauge P21 in the PFDA-GW for the HydroM2D model. Different colors represent different particles.

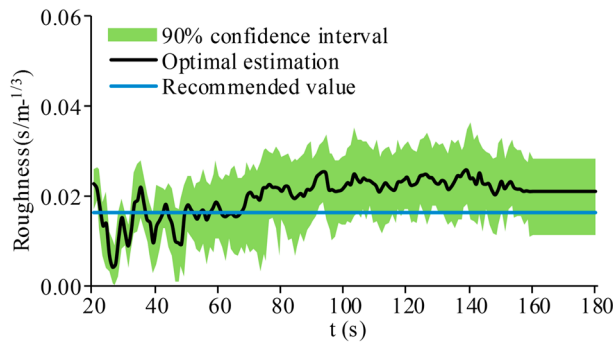


Figure 14. The 90% confidence intervals of the Manning's roughness coefficients at the whole computational domain derived from the PFDA-GW for the HydroM2D model.

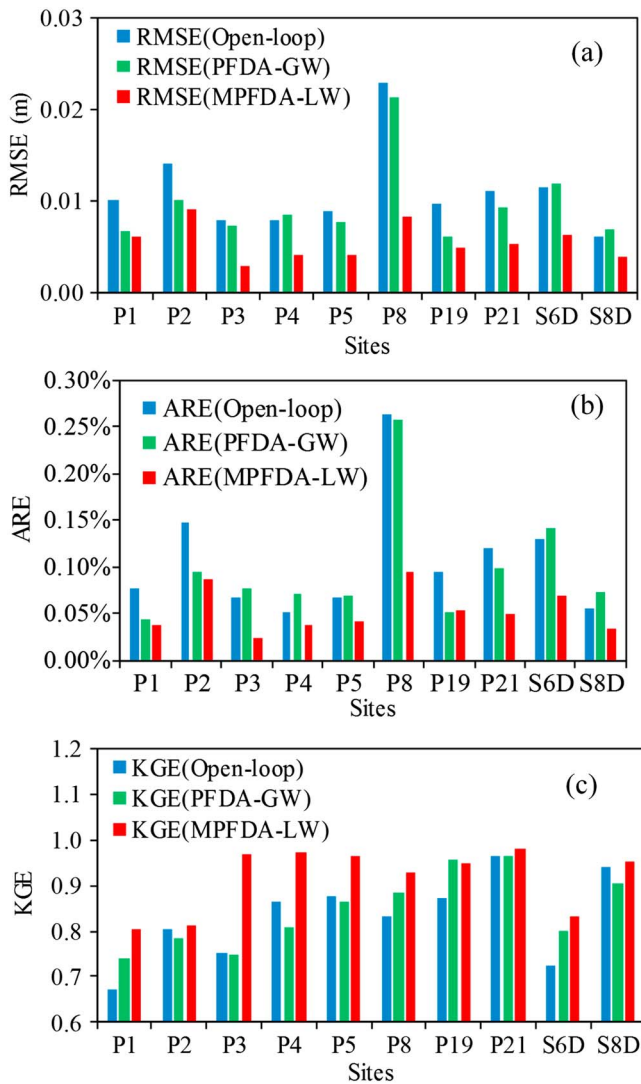


Figure 15. RMSEs (a), AREs (b), and KGEs (c) of assimilated water stages derived from the MPFDA-LW and the PFDA-GW for the HydroM2D model and simulated water stages derived from the open-loop simulations against observed water stages at the 10 gauges.

3.5. Comparison of the Performances of the MPFDA-LW and the PFDA-GW for the HydroM2D Model

The RMSEs, AREs, and KGEs of assimilated water stages derived by the MPFDA-LW, the PFDA-GW, and the open-loop simulations at the 10 gauges are shown in Figure 15. Compared to the open-loop simulations, the MPFDA-LW could significantly improve the performance of the HydroM2D in simulating dam-break flood inundation at all 10 gauges. However, the PFDA-GW could not improve the performance of the HydroM2D model in simulating the water stages at each gauge. The RMSEs and AREs of the assimilated water stages derived from the PFDA-GW for the HydroM2D model at several gauges were greater than those derived from open-loop simulations (e.g., gauges P4, S6D, and S8D). The results indicated that the MPFDA-LW for the HydroM2D model considering spatial-temporal variability of Manning's roughness coefficients was more suitable for simulating and predicting flood inundation.

3.6. Discussion

The MPFDA-LW for the HydroM2D model considering the spatial-temporal variability of Manning's roughness coefficients showed the good performance in simulating and predicting water stages at different gauges through simultaneously updating corresponding Manning's roughness coefficients with water stage assimilation. By contrast, Xu et al. (2017) and Y. Kim et al. (2013) only adopted different Manning's roughness coefficients at some separated zones (e.g., river channel, floodplain, and the area colonized by trees) and the global weighting procedure (Giustarini et al., 2011) to update the weights of particles. The PF-based data assimilation method aimed to achieve balanced model performances at several hydrological stations simultaneously. Therefore, in order to reach a global optimum, the performances of the PF-based data assimilation method at any individual cross section or computational grid cells were sacrificed. In addition, Giustarini et al. (2011) and Matgen et al. (2010) adopted constant Manning's roughness coefficients in the PF-based data assimilation method for 1-D model. Flow conditions of dam-break flood often dramatically varies within a short time, so the Manning's roughness coefficients at different areas with different geography, underlying surfaces, and flow conditions vary with dam-break flood inundation (Xu et al., 2017). Therefore, it is difficult to improve the performance of 2-D hydrodynamic models in the simulation of dam-break flood inundation with existing PF-based data assimilation methods.

The assimilation effects of the MPFDA-LW for the HydroM2D model could be propagate in the temporal dimension, but the assimilation effects were difficult to be propagate in the spatial dimension due to the particular local weighting procedure adopted in the MPFDA-LW. Actually, in the procedure, only the weights of particles at the grid cells with gauges were updated based on the likelihoods between simulated stages with observed stages. Therefore, the influences of assimilation were limited to the grid cells with gauges. Other localized PFs might enhance the influences of assimilation in the spatial dimension (Penny & Miyoshi, 2016; Poterjoy, 2016; Poterjoy et al., 2019). In these localized PFs, the grid cells around the observation gauges were considered as a single block of N particles. The states of the block were subjected to the same update according to the observation. The performances of the localized PF-based data assimilation methods for hydrodynamic models should be further explored.

In the study, we demonstrated that the MPFDA-LW for the HydroM2D model with a high assimilation accuracy was suitable for simulating and predicting flood inundation. It also had the potential in improving the performance of hydrodynamic models in simulation and prediction of hydrodynamic processes with complex geography and underlying surfaces. A flood flow generally significantly varies within a short time compared to the relatively stable flow in river basins and lakes, so inflow boundary conditions and water stages in the Toce River physical model were observed frequently (per second). The high observation frequency provided the condition of high assimilation frequency. In practice, the assimilation frequency of the MPFDA-LW for hydrodynamic models for a specific scenario should be determined according to application requirements and observation conditions. With the upcoming Surface Water Ocean Topography mission and the development of wireless sensor monitoring systems (e.g., automatic hydrological monitoring station), more available global observations of water stages with a high accuracy can be used to improve the simulation and prediction abilities of hydrodynamic models with the MPFDA-LW.

4. Conclusions

In this study, we proposed a modified PF-based data assimilation method with the local weighting procedure (MPFDA-LW) for a 2-D hydrodynamic model (HydroM2D) considering the spatial-temporal variability of Manning's roughness coefficients. In addition, another PF-based data assimilation with the global weighting procedure (PFDA-GW) for the HydroM2D with the spatially uniform Manning's roughness coefficient was adopted. The performances of the MPFDA-LW and the PFDA-GW for the HydroM2D in simulating dam-break flood inundation in the physical model of Toce River were evaluated and compared. In the MPFDA-LW and the PFDA-GW, observed water stages were assimilated into the HydroM2D model to simultaneously adjust simulated water stages and update Manning's roughness coefficients.

The MPFDA-LW could simultaneously improve the performances of the HydroM2D model in simulating and predicting water stages at all the 10 gauges through updating Manning's roughness coefficients. By contrast, the PFDA-GW could not improve the performances of the HydroM2D model in simulating water stages at most gauges. Overall, the MPFDA-LW had the higher potential in improving the performance of hydrodynamic models in simulating and predicting flood inundation and hydrodynamic processes in river basins and lakes.

The 90% confidence intervals of assimilated water stages at 10 gauges derived by the MPFDA-LW for the HydroM2D model could not entirely involve the observed water stages because the PF-based data assimilation method only considered the uncertainties associated with Manning's roughness coefficients and inflow conditions. In order to further improve the performance of the PF-based data assimilation, other uncertainties from input data (e.g., river-bed geometry) and model structures (e.g., governing equations and numerical computation method) should be considered in the PF-based data assimilation in the future (Moradkhani, Hsu, et al., 2005; Xu et al., 2017).

Acknowledgments

This work was jointly supported by the National Key Research and Development Program of China (2017YFC0405804 and 2017YFC0405801), the National Natural Science Foundation of China (51309254 and 51579248), the Key Scientific Research Project of China Institute of Water Resources and Hydropower Research (WR0145B272016), and Open Research Fund of State Key Laboratory of Simulation and Regulation of Water Cycle in River Basin, China Institute of Water Resources and Hydropower Research (IWHR-SKL-201517). Data and Fortran 90 source codes to reproduce the analyses in this study are available on figshare at <https://doi.org/10.6084/m9.figshare.6721568.v1>. We acknowledge Frazão for kindly sharing the data of Toce River physical model. We also would like to thank three anonymous referees for their helpful and constructive comments and suggestions.

References

- Aureli, F., Mignosa, P., & Tomirotti, M. (2000). Numerical simulation and experimental verification of dam-break flows with shocks. *Journal of Hydraulic Research*, 38(3), 197–206. <https://doi.org/10.1080/00221680009498337>
- Biancamaria, S., Durand, M., Andreadis, K. M., Bates, P. D., Boone, A., Mognard, N. M., et al. (2011). Assimilation of virtual wide swath altimetry to improve Arctic river modeling. *Remote Sensing of Environment*, 115(2), 373–381. <https://doi.org/10.1016/j.rse.2010.09.008>
- Burgers, G., Jan van Leeuwen, P., & Evensen, G. (1998). Analysis scheme in the ensemble Kalman filter. *Monthly Weather Review*, 126(6), 1719–1724. [https://doi.org/10.1175/1520-0493\(1998\)126<1719:ASITEK>2.0.CO;2](https://doi.org/10.1175/1520-0493(1998)126<1719:ASITEK>2.0.CO;2)
- Camacho, R. A., Martin, J. L., McAnally, W., Diaz-Ramirez, J., Rodriguez, H., Sucsy, P., & Zhang, S. (2015). A comparison of Bayesian Methods for uncertainty analysis in hydraulic and hydrodynamic modeling. *Journal of the American Water Resources Association*, 51(5), 1372–1393. <https://doi.org/10.1111/1752-1688.12319>
- Cao, Y., Ye, Y., Liang, L., Jiang, Y., Zhao, H., Wang, H., & Yan, D. (2017). Numerical simulation of dam-break flow based on structured grids. *Advances in Water Science*, 28(6), 868–878.
- Chávarri, E., Crave, A., Bonnet, M.-P., Mejía, A., Santos Da Silva, J., & Guyot, J. L. (2013). Hydrodynamic modelling of the Amazon River: Factors of uncertainty. *Journal of South American Earth Sciences*, 44, 94–103. <https://doi.org/10.1016/j.jsames.2012.10.010>
- Coraci, E., Umgiesser, G., & Zonta, R. (2007). Hydrodynamic and sediment transport modelling in the canals of Venice (Italy). *Estuarine, Coastal and Shelf Science*, 75(1-2), 250–260. <https://doi.org/10.1016/j.ecss.2007.02.028>
- Giustarini, L., Matgen, P., Hostache, R., Montanari, M., Plaza, D., Pauwels, V. R. N., et al. (2011). Assimilating SAR-derived water level data into a hydraulic model: A case study. *Hydrology and Earth System Sciences*, 15(7), 2349–2365. <https://doi.org/10.5194/hess-15-2349-2011>
- Gordon, N. J., Salmond, D. J., & Smith, A. F. M. (1993). Novel approach to nonlinear/non-Gaussian Bayesian state estimation. *IEE Proceedings F - Radar and Signal Processing*, 140(2), 107–113. <https://doi.org/10.1049/ip-f-2.1993.0015>

- Gupta, H. V., Kling, H., Yilmaz, K. K., & Martinez, G. F. (2009). Decomposition of the mean squared error and NSE performance criteria: Implications for improving hydrological modelling. *Journal of Hydrology*, *377*(1-2), 80–91. <https://doi.org/10.1016/j.jhydrol.2009.08.003>
- Han, X., & Li, X. (2008). An evaluation of the nonlinear/non-Gaussian filters for the sequential data assimilation. *Remote Sensing of Environment*, *112*(4), 1434–1449. <https://doi.org/10.1016/j.rse.2007.07.008>
- Kim, K., Park, M., Min, J.-H., Ryu, I., Kang, M.-R., & Park, L. J. (2014). Simulation of algal bloom dynamics in a river with the ensemble Kalman filter. *Journal of Hydrology*, *519*, 2810–2821. <https://doi.org/10.1016/j.jhydrol.2014.09.073>
- Kim, Y., Tachikawa, Y., Shiiba, M., Kim, S., Yorozu, K., & Noh, S. J. (2013). Simultaneous estimation of inflow and channel roughness using 2D hydraulic model and particle filters. *Journal of Flood Risk Management*, *6*(2), 112–123. <https://doi.org/10.1111/j.1753-318X.2012.01164.x>
- Lai, W., & Khan, A. A. (2012). A discontinuous Galerkin method for two-dimensional shallow water flows. *International Journal for Numerical Methods in Fluids*, *70*(8), 939–960. <https://doi.org/10.1002/fld.2721>
- Liang, D. F., Lin, B., & Falconer, R. A. (2007). Simulation of rapidly varying flow using an efficient TVD-MacCormack scheme. *International Journal for Numerical Methods in Fluids*, *53*(5), 811–826. <https://doi.org/10.1002/fld.1305>
- Liang, Q., Borthwick, A. G. L., & Stelling, G. (2004). Simulation of dam- and dyke-break hydrodynamics on dynamically adaptive quadtree grids. *International Journal for Numerical Methods in Fluids*, *46*(2), 127–162. <https://doi.org/10.1002/fld.748>
- Liang, Q. H., & Borthwick, A. G. L. (2009). Adaptive quadtree simulation of shallow flows with wet-dry fronts over complex topography. *Computers & Fluids*, *38*(2), 221–234. <https://doi.org/10.1016/j.compfluid.2008.02.008>
- Liang, Q. H., Zang, J., Borthwick, A. G. L., & Taylor, P. H. (2007). Shallow flow simulation on dynamically adaptive cut cell quadtree grids. *International Journal for Numerical Methods in Fluids*, *53*(12), 1777–1799. <https://doi.org/10.1002/fld.1363>
- Mao, J., Zhao, L., Bai, X., Guo, B., Liu, Z., & Li, T. (2016). A novel well-balanced scheme for modeling of dam break flow in drying-wetting areas. *Computers & Fluids*, *136*, 324–330. <https://doi.org/10.1016/j.compfluid.2016.06.022>
- Marsoli, R., & Wu, W. (2014). 3-D finite-volume model of dam-break flow over uneven beds based on VOF method. *Advances in Water Resources*, *70*, 104–117. <https://doi.org/10.1016/j.advwatres.2014.04.020>
- Matgen, P., Montanari, M., Hostache, R., Pfister, L., Hoffmann, L., Plaza, D., et al. (2010). Towards the sequential assimilation of SAR-derived water stages into hydraulic models using the particle filter: Proof of concept. *Hydrology and Earth System Sciences*, *14*(9), 1773–1785. <https://doi.org/10.5194/hess-14-1773-2010>
- Mattern, J. P., Dowd, M., & Fennel, K. (2013). Particle filter-based data assimilation for a three-dimensional biological ocean model and satellite observations. *Journal of Geophysical Research: Oceans*, *118*, 2746–2760. <https://doi.org/10.1002/jgrc.20213>
- Moradkhani, H., Hsu, K., Gupta, H., & Sorooshian, S. (2005). Uncertainty assessment of hydrologic model states and parameters: Sequential data assimilation using the particle filter. *Water Resources Research*, *41*, W05012. <https://doi.org/10.1029/2004WR003604>
- Moradkhani, H., Sorooshian, S., Gupta, H. V., & Houser, P. R. (2005). Dual state-parameter estimation of hydrological models using ensemble Kalman filter. *Advances in Water Resources*, *28*(2), 135–147. <https://doi.org/10.1016/j.advwatres.2004.09.002>
- Neal, J., Schumann, G., Bates, P., Buytaert, W., Matgen, P., & Pappenberger, F. (2009). A data assimilation approach to discharge estimation from space. *Hydrological Processes*, *23*(25), 3641–3649. <https://doi.org/10.1002/hyp.7518>
- Neal, J. C., Atkinson, P. M., & Hutton, C. W. (2007). Flood inundation model updating using an ensemble Kalman filter and spatially distributed measurements. *Journal of Hydrology*, *336*(3-4), 401–415. <https://doi.org/10.1016/j.jhydrol.2007.01.012>
- Pasetto, D., Camporese, M., & Putti, M. (2012). Ensemble Kalman filter versus particle filter for a physically-based coupled surface-subsurface model. *Advances in Water Resources*, *47*(10), 1–13. <https://doi.org/10.1016/j.advwatres.2012.06.009>
- Penna, I. M., Derron, M.-H., Volpi, M., & Jaboyedoff, M. (2013). Analysis of past and future dam formation and failure in the Santa Cruz River (San Juan province, Argentina). *Geomorphology*, *186*, 28–38. <https://doi.org/10.1016/j.geomorph.2012.12.011>
- Penny, S. G., & Miyoshi, T. (2016). A local particle filter for high-dimensional geophysical systems. *Nonlinear Processes in Geophysics*, *23*(6), 391–405. <https://doi.org/10.5194/npg-23-391-2016>
- Plaza, D. A., De Keyser, R., De Lannoy, G. J. M., Giustarini, L., Matgen, P., & Pauwels, V. R. N. (2012). The importance of parameter resampling for soil moisture data assimilation into hydrologic models using the particle filter. *Hydrology and Earth System Sciences*, *16*(2), 375–390. <https://doi.org/10.5194/hess-16-375-2012>
- Poterjoy, J. (2016). A localized particle filter for high-dimensional nonlinear systems. *Monthly Weather Review*, *144*(1), 59–76. <https://doi.org/10.1175/MWR-D-15-0163.1>
- Poterjoy, J., Wicker, L., & Buehner, M. (2019). Progress toward the application of a localized particle filter for numerical weather prediction. *Monthly Weather Review*, *147*(4), 1107–1126. <https://doi.org/10.1175/MWR-D-17-0344.1>
- Prestininzi, P. (2008). Suitability of the diffusive model for dam break simulation: Application to a CADAM experiment. *Journal of Hydrology*, *361*(1-2), 172–185. <https://doi.org/10.1016/j.jhydrol.2008.07.050>
- Qi, L., Ma, R., Hu, W., & Loisel, S. A. (2014). Assimilation of MODIS chlorophyll-*a* data into a coupled hydrodynamic-biological model of Taihu Lake. *IEEE Journal of Selected Topics in Applied Earth Observations and Remote Sensing*, *7*(5), 1623–1631. <https://doi.org/10.1109/jstars.2013.2280815>
- Qin, J., Liang, S., Yang, K., Kaihotsu, I., Liu, R., & Koike, T. (2009). Simultaneous estimation of both soil moisture and model parameters using particle filtering method through the assimilation of microwave signal. *Journal of Geophysical Research*, *114*, D15103. <https://doi.org/10.1029/2008JD011358>
- Rueda, F., Vidal, J., & Schladow, G. (2009). Modeling the effect of size reduction on the stratification of a large wind-driven lake using an uncertainty-based approach. *Water Resources Research*, *45*, W03411. <https://doi.org/10.1029/2008WR006988>
- Schneider, R., Ridler, M. E., Godiksen, P. N., Madsen, H., & Bauer-Gottwein, P. (2018). A data assimilation system combining CryoSat-2 data and hydrodynamic river models. *Journal of Hydrology*, *557*, 197–210. <https://doi.org/10.1016/j.jhydrol.2017.11.052>
- Sehnert, C., Huang, S., & Lindenschmidt, K. E. (2009). Quantifying structural uncertainty due to discretisation resolution and dimensionality in a hydrodynamic polder model. *Journal of Hydroinformatics*, *11*(1), 19–30. <https://doi.org/10.2166/hydro.2009.038b>
- Snyder, C., Bengtsson, T., Bickel, P., & Anderson, J. (2008). Obstacles to high-dimensional particle filtering. *Monthly Weather Review*, *136*(12), 4629–4640. <https://doi.org/10.1175/2008MWR2529.1>
- Soares Frazão, S. (1999). The Toce River test case: Numerical results analysis. Paper presented at the Proceedings of the 3rd CADAM Workshop, Milan, Italy.
- Teng, J., Jakeman, A. J., Vaze, J., Croke, B. F. W., Dutta, D., & Kim, S. (2017). Flood inundation modelling: A review of methods, recent advances and uncertainty analysis. *Environmental Modelling & Software*, *90*, 201–216. <https://doi.org/10.1016/j.envsoft.2017.01.006>
- Thompson, A., Guo, Y., & Moin, S. (2008). Uncertainty analysis of a two-dimensional hydrodynamic model. *Journal of Great Lakes Research*, *34*(3), 472–484. [https://doi.org/10.3394/0380-1330\(2008\)34\[472:UAOATH\]2.0.CO;2](https://doi.org/10.3394/0380-1330(2008)34[472:UAOATH]2.0.CO;2)

- Van Leeuwen, P. J. (2009). Particle filtering in geophysical systems. *Monthly Weather Review*, *137*(12), 4089–4114. <https://doi.org/10.1175/2009MWR2835.1>
- Warmink, J. J., Booij, M. J., Hulscher, S. J. M. H., Klis, V. D. H., & Dittrich, A. (2010). Uncertainty in design water levels due to uncertain bed form roughness in the river Rhine. Paper presented at the River Flow 2010.
- West, M. (1993). Mixture models, Monte Carlo, Bayesian updating and dynamic models. *Computer Science & Statistics*, *25*, 1–11.
- Xu, X. Y., Zhang, X. S., Fang, H. W., Lai, R. X., Zhang, Y. F., Huang, L., & Liu, X. B. (2017). A real-time probabilistic channel flood-forecasting model based on the Bayesian particle filter approach. *Environmental Modelling & Software*, *88*, 151–167. <https://doi.org/10.1016/j.envsoft.2016.11.010>
- Ye, Z., & Zhao, X. (2017). Investigation of water-water interface in dam break flow with a wet bed. *Journal of Hydrology*, *548*, 104–120. <https://doi.org/10.1016/j.jhydrol.2017.02.055>
- Zhang, H. J., Qin, S. X., Ma, J. W., & You, H. J. (2013). Using residual resampling and sensitivity analysis to improve particle filter data assimilation accuracy. *IEEE Geoscience and Remote Sensing Letters*, *10*(6), 1404–1408. <https://doi.org/10.1109/lgrs.2013.2258888>
- Zhang, S., Yuan, R., Wu, Y., & Yi, Y. (2017). Parallel computation of a dam-break flow model using OpenACC applications. *Journal of Hydraulic Engineering*, *143*(1), 04016070. [https://doi.org/10.1061/\(asce\)hy.1943-7900.0001225](https://doi.org/10.1061/(asce)hy.1943-7900.0001225)